Frequency Selective Surface With Quasi-Elliptic Bandpass Response Using Radiation Null of Patch Antenna

Yin Li, Sai-Wai Wong, *Senior Member, IEEE*, Shiyan Wang, *Member, IEEE*, Jing-Yu Lin, Baiyang Liu, Lei Zhu, *Fellow, IEEE*, and Yejun He, *Senior Member, IEEE*

***Abstract*—A novel design of bandpass frequency selective surface (FSS) with high selectivity is proposed based on the antenna-filter-antenna (AFA) concept. Traditional AFA-based FSSs improve filtering performance by adding the order of resonator or the coupling paths. On account of the reciprocity theorem, transmission zeros are here introduced by the antenna's radiation null. The proposed FSS consists of two patch antennas connected with one pin and a C-type slot on the ground. The aforementioned structure generates two controllable radiation nulls related to the lengths of slots without any extra circuits. Therefore, two transmission zeros at both edges of the passband can be controlled by adjusting the dimension of slots. A prototype is fabricated and measured. Numerical simulation and measured results are in good agreement, which demonstrates that the proposed AFA-based FSS exhibits a quasi-elliptic bandpass response and a low profile.**

***Index Terms*—Fast roll-off, frequency selective surface (FSS), high-frequency selectivity, radiation null, transmission zeros (TZs).**

I. Introduction

FREQUENCY selective surfaces (FSSs) work as a spatial filter, which can be generally used in antenna radomes [1], [2], absorbers [3], polarization [4], antenna lens [5], and so on. In practical applications, a bandpass FSS with sharp roll-off and low profile is desired.

Traditional FSSs are comprised of a 2-D periodic array of the patches or apertures printed on a single layer. These FSSs exhibit a first-order filter response, suffering from a very poor filtering performance. A good filtering performance can be achieved by using high-order filter, which can be realized by cascading a variety of single-layer structures to form a multilayer structure [6]–[8]. In [6], a third-order FSS consisted of three-layer metal structures was designed to obtain one transmission zero (TZ). In [7], an FSS with two TZs at both sides of the passband was presented. These two TZs were realized by the extra inductor in the resonators. A high-selectivity filtering response can also be attained by cascading 2-D FSS with two dielectric layers and an air spacer [9]. It unavoidably results in a large thickness and complex multilayer structures when the operating frequency is low.

Similar to microwave filter, the multiple-path coupling is employed to design the FSS with a quasi-elliptic response. In [10] and [11], several FSSs with quasi-elliptic filtering performance were proposed, in which the electric and magnetic coupling paths were introduced by the coupling apertures. The concept of 3-D FSSs was reported to obtain a high filtering performance [12]–[15]. Several 3-D FSSs based on substrate-integrated waveguides (SIWs) cavities located in different layers were proposed in [12] and [13]. The quasi-elliptic bandpass response can be realized by the cross coupling between the SIW cavity modes. A category of 3-D FSSs is composed of microstrip line or slotline with 2-D periodic configuration, in which the TEM modes can be used to obtain the high filtering performance and control frequency response [16]–[20]. With the help of multimode resonators, good out-of-band performances, such as high selectivity and harmonic suppression, can be achieved [19], [20].

The antenna-filter-antenna concept is proposed to realize the FSSs with bandpass filtering response from the view of antenna. An FSS based on two patches coupled with an aperture was presented in [21]. The transmission zero can be also achieved by increasing the coupling paths [22]. This concept has also been used to design lens [5], polarization converter [23], [24], and transmit array [25], [26].

In this letter, an AFA-based FSS with two controllable transmission zeroes is proposed. Unlike the previous works, the proposed FSS is designed in view of the radiation null of antenna. Furthermore, the patch antenna without an extra circuit is first introduced in FSS for quasi-elliptic bandpass response [27]–[29]. The proposed FSS possesses high selectivity without

Manuscript received September 8, 2020; revised October 9, 2020 and October 31, 2020; accepted October 31, 2020. Date of publication November 6, 2020; date of current version January 14, 2021. This work was supported in part by the Shenzhen Science and Technology Programs under Grant JCYJ20190808145411289 and Grant JCYJ20180305124543176, in part by the Natural Science Foundation of Guangdong Province under Grant 2018A030313481, in part by Shenzhen University Research Startup Project of New Staff under Grant 860-000002110311, in part by Guangdong Basic and Applied Basic Research Foundation under Grant 2019A1515111166 and Grant 2019A1515111127, in part by China Postdoctoral Science Foundation under Grant 2019M652893 and Grant 2020M682876, and in part by the Natural Science Foundation of China under Grant 62071306. *(Corresponding author: Sai-Wai Wong.)*

Yin Li, Sai-Wai Wong, Baiyang Liu, and Yejun He are with the College of Electronics and Information Engineering, Shenzhen University, Shenzhen 518060, China (e-mail: liyinuestc@gmail.com; wongsaiwai@ieee.org; lby234256557@vip.qq.com; heyejun@126.com).

Shiyan Wang is with the Jiangsu Key Laboratory of 3D Printing Equipment and Manufacturing, School of Electrical and Automation Engineering, Nanjing Normal University, Nanjing 210046, China (e-mail: nustwang@163.com).

Jing-Yu Lin is with the School of Electrical and Data Engineering, University of Technology Sydney, Ultimo, NSW 2007, Australia (e-mail: l.j.2014@ieee.org).

Lei Zhu is with the Department of Electrical and Computer Engineering, Faculty of Science and Technology, University of Macau, Macau 999078, China (e-mail: leizhu@umac.mo).

Digital Object Identifier 10.1109/LAWP.2020.3036119

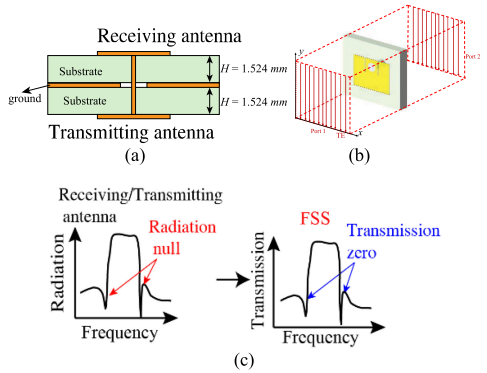

Fig. 1. Topology of the FSS with quasi-elliptic bandpass response. (a) Topology of the antenna-filter-antenna-based FSS. (b) FSS with TE mode excited. (c) Work principle of transmission zero.

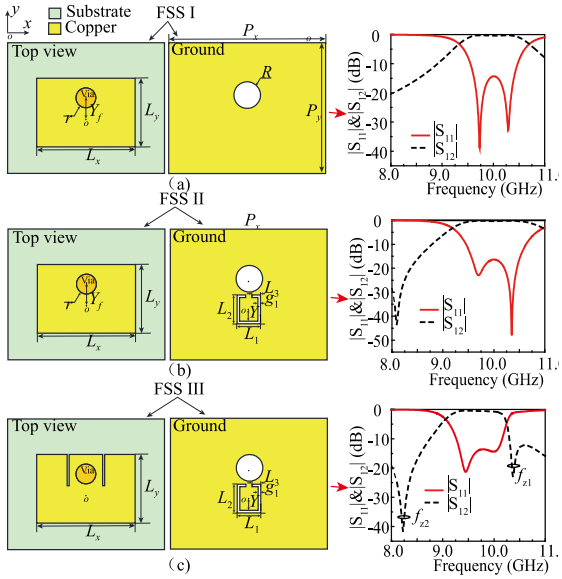

Fig. 2. Layout of three different AFA-based FSS with these frequency responses. (a) FSS I with frequency response. (b) FSS II with frequency response. (c) FSS III (proposed) with frequency response.

extra complex circuit and multilayer structure, which is easily fabricated.

II. Design of the Proposed FSS

In Fig. 1(a), the topology of a unit cell in FSS is illustrated, where a pair of antennas serves as receiver and transmitter, respectively. The pin between them can be considered as a matching network. Polarization direction of the incident wave is shown in Fig. 1(b). The receiving and transmitting antennas have two radiation nulls located on both sides of the operating passband. Based on the reciprocity theorem, the proposed FSS consisted of two antennas which can achieve two TZs at both sides of passband, as shown in Fig. 1(c).

Three FSSs, named FSS I, FSS II, FSS III, are illustrated in Fig. 2, which consists of three different patch antennas, called as antenna I, II, and III. All these three AFA-based FSSs are designed on Rogers RO4003C with relative permittivity of 3.55, loss tangent of 0.0027, and a thickness of 1.524 mm. A Rogers RO4450F bonding film with relative permittivity of 3.55, loss

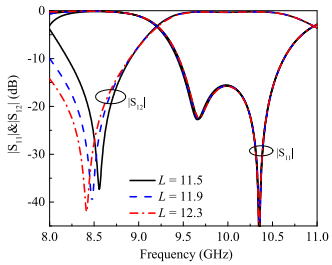

Fig. 3. Simulated lower transmission zero under different length of slot on ground (L) ($\theta = 0°$) with $L_{s1} = 0$, P_x =18, $P_y = 14$, $Y_1 = 3.0$, $r = 0.8$, R= 1.0, $L_x = 10$, $L_y = 7$ (all in mm).

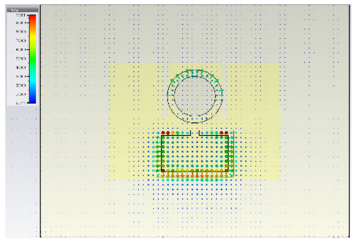

Fig. 4. Electric field on ground of TZ at lower frequency.

tangent of 0.004, and a thickness of 0.1 mm is used to adhere two RO4003C dielectric substrates.

As shown in Fig. 2(a), the two conventional patches are connected by a via-hole to realize an AFA-based FSS. The dimension of the FSS I is with $P_x = 18$, $P_y = 14$, $Y_f = 1.5$, $r = 0.8$, $R = 1.0$, $L_x = 10$, $L_y = 7$ (all in mm). Its frequency responses under the normal incidence are also shown in Fig. 2(a). Bandpass filtering frequency response and good transmission in the passband are obtained. However, the slow roll-offs of the transmission coefficients $|S_{21}|$ at the two edges of passband are slow and thus the out-of-band rejection is poor. Since antenna I is the traditional patch antenna, without frequency selectivity and radiation null. To improve the selectivity of AFA-based FSS, radiation null needs to be introduced in patch antenna, according to the topology of FSS depicted in Fig. 1(c).

Based on FSS I, an extra C-slot is introduced on ground to construct the FSS II, as shown in Fig. 2(b). In this context, C-slot works as a notched band to provide a transmission zero at low frequency. The frequency of the transmission zero is related to the length of the slot [31]

$$f_L = \frac{C}{2L * \sqrt{\varepsilon_{\text{eff}}}} \tag{1}$$

where $L = L_1 + L_2{*}2{+}L_3 {*}2$, represents the total length of C-slot.

As shown in Fig. 3, it can be also discovered that the transmission zero will be shifted when the length of L is changed. This is because the slot is in half-wavelength resonance, and the frequency of the notch band is related to the total length of the C-slot. Moreover, reflection coefficient keeps relative stable, which verifies that the lower TZ is adjustable with little influence on reflection coefficient. The lower TZ leads to a boresight radiation null. To give more physical insight into the underlying mechanism, the field distribution at the frequency of lower TZ is shown in Fig. 4. It can be found that the electromagnetic field mainly focuses in C slot. Besides, as shown in Fig. 5, the location

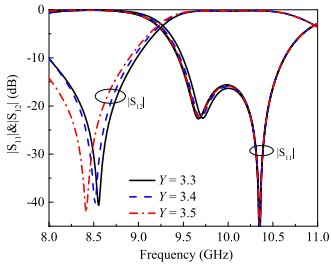

Fig. 5. Simulated lower transmission zero under different length of slot on ground (L) ($\theta = 0°$) with $L_{s1} = 0$, P_x =18, $P_y = 14$, $Y_1 = 3.0$, $r = 0.8$, R= 1.0, $L = 11.9$, $L_x = 10$, $L_y = 7$ (all in mm).

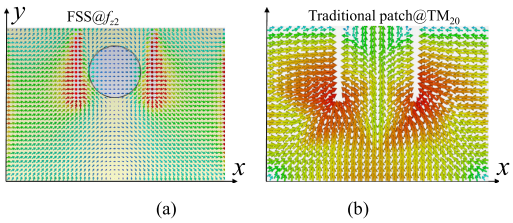

Fig. 6. (a) Tangential magnetic field on the patch at the f_{z2} in Fig. 3. (b) Tangential magnetic field of TM $_{20}$ mode on traditional the patch with two slot.

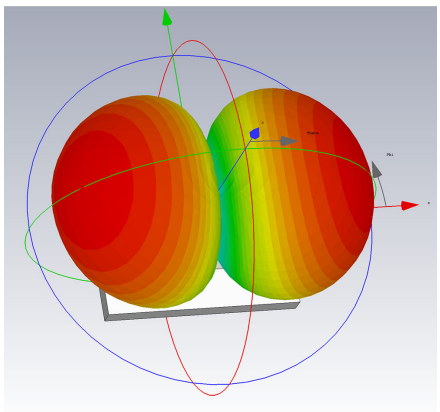

Fig. 7. Three-dimensional radiation pattern of TM_{20} on patch with slot.

of the C-slot (Y_1) also affects the f_{z1}, because the electronic field is different on the different positions of ground.

The FSS consisting of antenna III, called FSS III, can exhibit a quasi-elliptic response by optimizing the length of L_{s1} and L. The transmission and reflection coefficient of optimized FSS III are plotted in Fig. 2(c). Compared with FSS I, FSS III can provide better filtering frequency performance without any extra circuit and layer of structure, having the merits of simple structure and low profile.

For further explanation, the tangential magnetic field on the proposed patch at the upper TZ (f_{z2}) is plotted in Fig. 6(a). The tangential magnetic field of the TM_{20} mode on its counterpart radiator, a typical standalone probe-fed patch with two slots, at the upper TZ (f_{z2}) is plotted in Fig. 6(b). It can be found that the results between the proposed FSS unit and typical patch structures are similar to each other. Therefore, the TM_{20} mode of the patch is dominant at f_{z2}. The 3-D radiation pattern of TM_{20} on the typical patch with two slots is shown in Fig. 7. As we know, there is a boresight radiation null in the radiation pattern for TM_{20} mode. Consequently, the TE wave near the normal

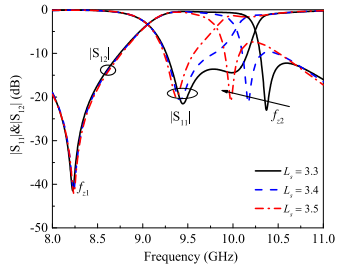

Fig. 8. Simulated *S*-parameters under different *Ls* (incident wave $\theta = 0°$) with P_x =18, $P_y = 14$, $Y_f = 1.5$, $Ls = 3.3$, $r = 1.2$, R= 1.6, $L_x = 10$, $L_y = 7$ (all in mm).

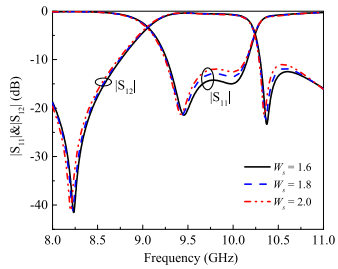

Fig. 9. *S*-parameter under various W_s , (incident wave $\theta = 0°$) with P_x =18, $P_y = 14$, $Y_f = 1.5$, $Ls = 3.3$, R= 1.0, $L_x = 10$, $L_y = 7$ (all in mm).

incidence cannot transmit through or be received by the FSS, and so the TZ of FSS is obtained.

As described in [32], the two slots on patch can reshape the current on patch thus manipulate the radiation patterns, and resonant frequencies of TM_{01} and TM_{20} modes under different slot lengths of the slot on patch (L_s) are provided in Table I. It can be found that the current, radiation pattern, and resonant frequency of TM_{01} mode in passband are nearly unchanged by L_s, since the slots are parallel to the current vectors and their perturbation is minimized. In contrast, the current of the TM_{20} mode is dramatically interrupted by the slots, since they are perpendicular to each other. When L_s is increased to 3.8 mm, the current distribution and radiation patterns even become similar and comparable to that of TM_{01} mode. Simultaneously, the resonant frequency decreases and boresight radiation null exists when L_s is less than 3.8 mm. Therefore, L_s can be used to control the TZ of proposed FSS by using radiation null. The upper TZ (f_{z2}) is decreased as the L_s increasing, as shown in Fig. 8.

The location of the slots on the patch (W_s) can affect the current of TM_{20} mode in different manner. It can also control the location of TZ. As shown in Table II, the resonant frequency of TM_{20} decreases with the increasing W_s. Therefore, the upper TZ of the proposed FSS is shifted to low frequency as W_s ascending. The transmission coefficients of the proposed FSS under various W_s are shown in Fig. 9. It can be discovered that the transmission zero is slightly shifted to lower frequency.

III. Fabrication and Measurement

The fabrication of the proposed FSS prototype is depicted in Fig. 10(a). The prototype consisted of 11×11 elements with a total size of 198 ×154 mm^2. Four elements are zoomed in to show the details, as shown in Fig. 10(a). For measurement, the FSS is placed in an anechoic chamber to avoid the interference

TABLE I
CURRENT, RADIATION PATTERN, RESONANT FREQUENCY OF TM_{01} AND TM_{20} MODE UNDER VARIOUS L_s WITH $W_s = 3.2$ mm

L_s (mm)	TM_{01} (10GHz)		TM_{20}		
	Current	Radiation pattern	Resonant frequency	Current	Radiation pattern
3.0	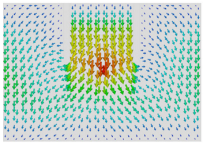	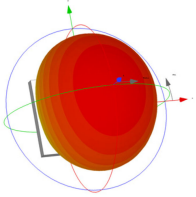	10.3 GHz	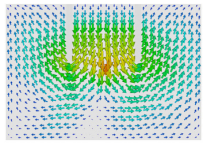	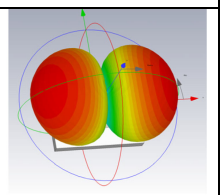
3.4	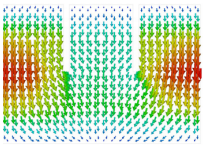	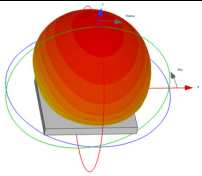	9.3 GHz	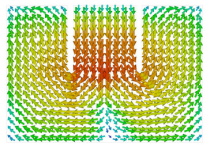	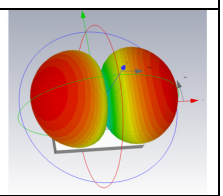
3.8	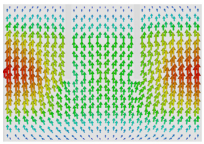	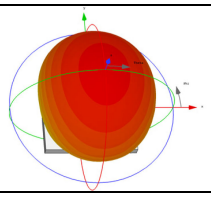	8.8 GHz	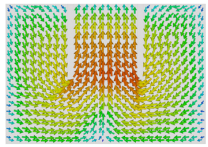	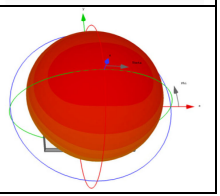

TABLE II
CURRENT, RADIATION PATTERN, RESONANT FREQUENCY OF TM_{20} UNDER VARIOUS W_s

L_s	$W_s = 1.6$ mm		$W_s = 1.8$ mm		$W_s = 2.0$ mm	
	Current	Resonant frequency	Current	Resonant frequency	Current	Resonant frequency
3.0	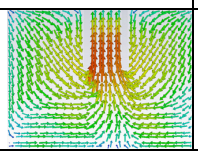	10.6 GHz	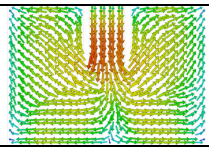	10.54GHz	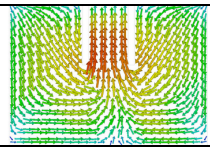	10.4GHz

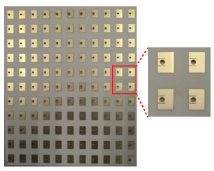

(a)

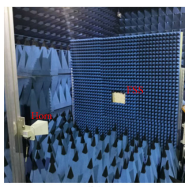

(b)

Fig. 10. Fabrication and the measured environment of the proposed AFA-based FSS. (a) Fabrication of proposed FSS. (b) Measurement environment.

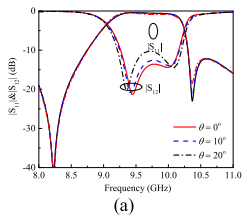

(a)

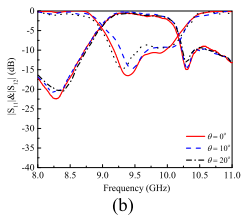

(b)

Fig. 11. Simulated and measured *S*-parameters of the proposed AFA-based FSS. (a) Simulated. (b) Measured.

signal, and the absorber is around it to absorb the edge diffraction waves, as shown in Fig. 10(b). Two horn antennas and a vector network analyzer are used in the measurement.

The simulated results under variable incidence angles are indicated in Fig. 11(a). It depicts the transmission coefficients keep stable in the passband and the frequencies of TZs are remained steady at both sides of passband with different incidence angles below 20°. The reflection coefficients are upward with the ascend of the angle of the incidence wave. In the range from 9.26 to 10.16 GHz, $|S_{11}|$ is less than –10 dB. Therefore, the bandwidth is about 9.25%. The measured results are plotted in Fig. 11(b). It can be found that the measured results relatively agree with the simulated ones. The TZs of the measured and simulated results express a good agreement.

IV. CONCLUSION

A novel AFA-based FSS with quasi-elliptic bandpass response has been proposed in this letter. In which, antenna with radiation null (filtering antenna) can be reused for the design of FSS. Since the radiation nulls of antenna without extra circuit, two transmission zeroes are obtained based on the reciprocity theorem. A prototype of AFA-based FSS is designed for demonstration, and the measurement results of the proposed FSS agree well with the simulated ones, which prove that the design method is feasible. Furthermore, this method can be extended to design FSS with high performance, such as high selectivity, wideband rejection, and so on, if a suitable antenna is adopted.

REFERENCES

[1] B. A. Munk, *Frequency Selective Surfaces: Theory and Design*. New York, NY, USA: Wiley, 2000.

[2] H. Chen, X. Hou, and L. Deng, "Design of frequency-selective surfaces radome for a planar slotted waveguide antenna," *IEEE Antennas Wireless Propag. Lett.*, vol. 8, pp. 1231–1233, 2009.

[3] A. K. Rashid, Z. Shen, and S. Aditya, "Wideband microwave absorber-based on a two-dimensional periodic array of microstrip lines," *IEEE Trans. Antennas Propag.*, vol. 58, no. 12, pp. 3913–3922, Dec. 2010.

[4] S. A. Winkler, W. Hong, M. Bozzi, and K. Wu, "Polarization rotating frequency selective surface based on substrate integrated waveguide technology," *IEEE Trans. Antennas Propag.*, vol. 58, no. 4, pp. 1202–1213, Apr. 2010.

[5] P. Xie, G. Wang, H. Li, J. Liang, and X. Gao, "Circularly polarized Fabry-Perot antenna employing a receiver-transmitter polarization conversion metasurface," *IEEE Trans. Antennas Propag.*, vol. 68, no. 4, pp. 3213–3218, Apr. 2020.

[6] M. Li and N. Behdad, "A third-order bandpass frequency selective surface with a tunable transmission null," *IEEE Trans. Antennas Propag.*, vol. 60, no. 4, pp. 2109–2113, Apr. 2012.

[7] N. Liu, X. Sheng, C. Zhang, and D. Guo, "Design and synthesis of bandpass frequency selective surface with wideband rejection and rast roll-off characteristics for radome applications," *IEEE Trans. Antennas Propag.*, vol. 68, no. 4, pp. 2975–2983, Apr. 2020.

[8] C. Jin, Q. Lv, J. Wang, and Y. Li, "Capped dielectric inserted perforated metallic plate bandpass frequency selective surface," *IEEE Trans. Antennas Propag.*, vol. 65, no. 12, pp. 7129–7136, Dec. 2017.

[9] B. Li and Z. Shen, "Synthesis of quasi-elliptic bandpass frequency-selective surface using cascaded loop arrays," *IEEE Trans. Antennas Propag.*, vol. 61, no. 6, pp. 3053–3059, Jun. 2013.

[10] D. S. Wang, B. J. Chen, P. Zhao, and C. H. Chan, "High selectivity frequency selective surfaces at millimeter-wave and terahertz frequencies," in *Proc. Global Millimeter-Waves Symp.*, May 2015, pp. 1–3.

[11] D. S. Wang, P. Zhao, and C. H. Chan, "Design and analysis of a high-selectivity frequency-selective surface at 60 GHz," *IEEE Trans. Microw. Theory Techn.*, vol. 64, no. 6, pp. 1694–1703, Jun. 2016.

[12] G. Q. Luo *et al.*, "Theory and experiment of novel frequency selective surface based on substrate integrated waveguide technology," *IEEE Trans. Antennas Propag.*, vol. 53, no. 12, pp. 4035–4043, Dec. 2005.

[13] G. Q. Luo, W. Hong, Q. H. Lai, K. Wu, and L. L. Sun, "Design and experimental verification of compact frequency-selective surface with quasi-elliptic bandpass response," *IEEE Trans. Microw. Theory Techn.*, vol. 55, no. 12, pp. 2481–2487, Dec. 2007.

[14] Z. Zhao *et al.*, "Bandpass FSS with zeros adjustable quasi-elliptic response," *IEEE Antennas Wireless Propag. Lett.*, vol. 18, no. 6, pp. 1184–1188, Jun. 2019.

[15] J. Zhu, W. Tang, C. Wang, C. Huang, and Y. Shi, "Dual-polarized bandpass frequency-selective surface with quasi-elliptic response based on square coaxial waveguide," *IEEE Trans. Antennas Propag.*, vol. 66, no. 3, pp. 1331–1339, Mar. 2018.

[16] A. K. Rashid, B. Li, and Z. Shen, "An overview of three-dimensional frequency-selective structures," *IEEE Antennas Propag. Mag.*, vol. 56, no. 3, pp. 43–67, Jun. 2014.

[17] B. Li and Z. Shen, "Three-dimensional bandpass frequency selective structures with multiple transmission zeros," *IEEE Trans. Microw. Theory Techn.*, vol. 61, no. 10, pp. 3589–3678, Oct. 2013.

[18] B. Li and Z. Shen, "Angular-stable and polarization-independent frequency selective structure with high selectivity," *Appl. Phys. Lett.*, vol. 103, no. 17, pp. 171607-1–171607-4, Oct. 2013.

[19] B. Li and Z. Shen, "Three-dimensional dual-polarized frequency selective structure with wide out-of-band rejection," *IEEE Trans. Antennas Propag.*, vol. 62, no. 1, pp. 130–137, Jan. 2014.

[20] B. Li and Z. Shen, "Bandpass frequency selective structure with wideband spurious rejection," *IEEE Antennas Wireless Propag. Lett.*, vol. 13, pp. 145–148, 2014.

[21] R. Pous and D. M. Pozar, "A frequency-selective surface using aperture coupled microstrip patches," *IEEE Trans. Antennas Propag.*, vol. 39,no. 12, pp. 1763–1769, Dec. 1991.

[22] A. Abbaspour, K. Sarabandi, and G. M. Rebeiz, "Antenna-filter-antenna arrays as a class of bandpass frequency selective surfaces," *IEEE Trans. Microw. Theory Techn.*, vol. 52, no. 8, pp. 1781–1789, Aug. 2004.

[23] B. Lin, J. Wu, X.-Y. Da, and J.-J. Ma, "A linear-to-circular polarization converter based on a second-order band-pass frequency selective surface," *Appl. Phys. A*, vol. 123, Dec. 2017, Art. no. 43.

[24] S. Wang, W. Liu, and W. Geyi, "Dual-band transmission polarization converter based on planar-dipole pair frequency selective surface," *Sci. Rep.*, vol. 8, Feb. 2018, Art. no. 3791.

[25] Q. Luo, S. Gao, M. Sobhy, X. Yang, Z.-Q. Cheng, and Y.-L. Geng., "A hybrid design method for thin-panel transmitarray antennas," *IEEE Trans. Antennas Propag.*, vol. 67, no. 10, pp. 6473–6483, Oct. 2019.

[26] Y. Cai *et al.*, "A novel ultrawideband transmitarray design using tightly coupled dipole elements," *IEEE Trans. Antennas Propag.*, vol. 67, no. 1, pp. 242–250, Jan. 2019.

[27] X. Y. Zhang, W. Duan, and Y.-M. Pan, "High-gain filtering patch antenna without extra circuit," *IEEE Trans. Antennas Propag.*, vol. 63, no. 12, pp. 5883–5888, Dec. 2015.

[28] Y. Zhang, X. Y. Zhang, L. Ye, and Y. Pan, "Dual-band base station array using filtering antenna elements for mutual coupling suppression," *IEEE Trans. Antennas Propag.*, vol. 64, no. 8, pp. 3423–3430, Aug. 2016.

[29] X. Y. Zhang, Y. Zhang, Y.-M. Pan, and W. Duan, "Low-profile dualband filtering patch antenna and its application to LTE MIMO system," *IEEE Trans. Antennas Propag.*, vol. 65, no. 1, pp. 103–113, Jan. 2017.

[30] J. Y. Jin, S. Liao, and Q. Xue, "Design of filtering-radiating patch antennas with tunable radiation nulls for high selectivity," *IEEE Trans. Antennas Propag.*, vol. 66, no. 4, pp. 2125–2130, Apr. 2018.

[31] D. Sarkar, K. V. Srivastava, and K. Saurav, "A compact microstrip-fed triple band-notched UWB monopole antenna," *IEEE Antennas Wireless Propag. Lett.*, vol. 13, pp. 396–399, 2014.

[32] F. Yang, X. X. Zhang, X. Ye, and Y. Rahmat-Samii, "Wideband E-shaped patch antennas for wireless communications," *IEEE Trans. Antennas Propag.*, vol. 49, no. 7, pp. 1094–1100, Jul. 2001.